Journal of Inorganic and Organometallic Polymers and Materials (2018) 28:2545–2553
https://doi.org/10.1007/s10904-018-0943-3

Preparation of Lignin-Based Hydrogel and Its Adsorption on Cu^{2+} Ions and Co^{2+} Ions in Wastewaters

Rongrong Tian[1] · Qing Liu[1] · Wei Zhang[1] · Yiyang Zhang[1]

Received: 7 May 2018 / Accepted: 1 August 2018 / Published online: 6 August 2018

Abstract
In the present study, we prepared a newly adsorbent, Chitosan (CTS) and sodium lignosulphonate (SLS) were added as monomers for the copolymerization of acrylic acid (AA), then ammonium persulfate (APS) bisacrylamide (NMBA) as a cross-linking agent, under the premise of ultrasound mixed uniformly prepared lignin-based hydrogel. The hydrogel samples were characterized by SEM, FT-IR and TG analysis. Finally, the samples were applied to the adsorption of heavy metal ions Cu^{2+} and Co^{2+}. The influences of external environmental factors such as pH value, adsorption time, adsorbent dosage and initial concentration of heavy metal ions on the adsorption process were discussed. It was found that the optimum pH value for the adsorption of two heavy metal ions was close to 6, and the adsorption kinetics was found to fit the pseudo-second-order model and the isotherm model was fitted to the Freundlich model. Among them, the adsorption capacity of Co^{2+} is 385 mg g^{-1} and Cu^{2+} is 290 mg g^{-1}.

Keywords Adsorption · Hydrogel · Sodium lignosulfonate · Heavy metal ions

1 Introduction

Heavy metal ions themselves have high toxicity, it will denature the protein, causing great harm to the health of plants and animals [1–4]. Heavy metal ions are non-biodegradable and have a cumulative effect, which causes great harm to the environment and human health. Through the enrichment of the food chain, heavy metal ions eventually reach the human body, destroying the activity of proteins and enzymes, affecting their function and causing diseases in humans. Studies have shown that serious diseases such as cancer, leukemia, dementia and even death can result even in low concentrations [5–10]. Therefore, the removal of heavy metal ions in wastewaters has become one of the major problems in the management of the environment in the world today. Its importance and necessity are unspeakable. Today there are many ways to remove heavy metal ions, such as chemical precipitation [11], ion exchange [12], membrane separation [13] and adsorption [14–20]. The above method to remove ions is still good, but most methods also exist a big flaw. There are secondary pollution, energy consumption, and complex operation. Adsorption is currently considered one of the best ways to treat heavy metal ions because of its low cost, ease of operation, and environmental friendliness, and high efficiency even at low concentrations. It is widely used to remove heavy metal ions from aqueous solutions. Adsorption of heavy metals wastewaters treatment, adsorption materials mainly concentrated in zeolite and diatomite and other inorganic adsorbents, functionalized porous materials, fibers and resins and other organic adsorbents and activated carbon and ash and other carbonaceous adsorbents [21]. However, the experimental cost is high, the separation is difficult, the reaction speed is slow, and the adsorption capacity of water samples with extremely high or very low concentration is limited [22, 23]. As a new type of polymer material with three-dimensional network structure, hydrogel have good water permeability, biocompatibility and degradability due to their ability to sense and respond to changes in environment, and can introduce different chelating groups as needed. Has been widely used in agriculture, forestry, horticulture, industry, agriculture, biomedicine, pharmacy and other fields [24–26]. As a new environmentally friendly adsorbent, hydrogel provide a new way to solve the problem of heavy metal ions pollution in water. As a highly effective absorbent gelling resin, preparation methods and

✉ Rongrong Tian
Tianrr922@126.com

[1] School of Environment and Safety Engineering, North University of China, Taiyuan 030051, Shanxi, China

adsorption properties of acrylic acid-acrylamide hydrogels have received much attention. However, the influence of external environment on their adsorption properties is still lack of systematic research. Temperature, pH, ionic strength and other external conditions can affect the hydrogel adsorption of heavy metal ions [27]. The reticular structure shows some excellent properties, which provides a convenient way to change the properties of natural polymer based materials [28, 29]. There are many ways to synthesize superabsorbent polymers, such as free radical solution polymerization [30], electrospinning [31] and reverse phase suspension polymerization [32]. Ultrasound synthesis with the advantages of being fast, simple and convenient to manipulate is considered an important and effective technique over other methods. Due to the advantages of the ultrasound synthesis method, more and more studies have been reported [33, 34]. At present, superabsorbent polymers have been widely used in various fields such as hygiene products [35], agriculture [36] and drug delivery systems [37, 38] and wastewater treatment [39, 40]. The aim of this experiment was to prepare excellent hydrogel by the excellent properties of sodium lignosulphonate, using a supra-assisted approach and by orthogonal optimization. Discussing the hydrogel swelling properties, including pH sensitivity, water retention and so on. In addition, to broaden the field of application, hydrogel serves as adsorbents for the adsorption of cobalt ions and copper ions and evaluates the adsorption effect as a function of contact time, solution pH and initial concentration.

2 Experimental

2.1 Materials

Chitosan (CTS, Hubei Yuancheng Pharmaceutical Co., Ltd.) was dissolved by magnetic stirring at 60 °C. Sodium lignosulfonate (SLS, Shanghai Tingruo Chemical Co., Ltd.) and acrylic acid (AA, Tianjin Dingshengxin Chemical Co., Ltd.) were polymers monomer. Ammonium persulfate (APS, Shanghai Suran Chemical Reagent Co., Ltd.) was as an initiator. *N*′*N*-Methylenebisacrylamide (NMBA, Sinopharm Chemical Reagent Co., Ltd, Shanghai, China) was as a cross-linking agent. The other agents in the experiment were purchased from Nanjing Chemical reagent Co., Ltd, such as Sodium hydroxide, Ethanol. All aqueous solutions used for polymerization reactions, swelling and adsorption study were prepared with deionized water.

2.2 Preparation of the Hydrogels

Ultrasound-assisted synthesis of hydrogels in this experiment: Weighing NaOH into the beaker in an ice-water bath and neutralize it by dropping AA, while the glass rod was constantly agitated in the process. Then CTS, SLS, NMBA and APS followed by adding to the solution, the full mixing. The mixture was then placed in a sonicator and the temperature was adjusted to 65 °C and the reaction was completed by sonication for 3 h. Finally, the resulting hydrogel was soaked in absolute ethanol for 24 h to remove unreacted monomers. The sample was dried to constant weight in a vacuum oven at 80 °C, and the dried sample was completely crushed to obtain the size of the object in the range of 40–60 mesh. The amounts of the above reagents were arranged according to the following orthogonal design Table 1. Figure 1 shows a schematic diagram of hydrogel synthesis.

Table 1 The 4-element 3-level orthogonal experiment design

$L_9(4^3)$	Factors			
	(A) CTS/g	(B) Initiator/g	(C) Cross-linker/g	(D) SLS/AA/%
1	A_1 0.1	B_1 0.0087	C_1 0.0011	D_1 4
2	A_1 0.1	B_2 0.0145	C_2 0.0017	D_2 6
3	A_1 0.1	B_3 0.0203	C_3 0.0023	D_3 8
4	A_2 0.2	B_1 0.0087	C_2 0.0017	D_3 8
5	A_2 0.2	B_2 0.0145	C_3 0.0023	D_1 4
6	A_2 0.2	B_3 0.0206	C_1 0.0011	D_2 6
7	A_3 0.3	B_1 0.0087	C_3 0.0023	D_2 6
8	A_3 0.3	B_2 0.0145	C_1 0.0011	D_3 8
9	A_3 0.3	B_3 0.0203	C_2 0.002	D_1 4

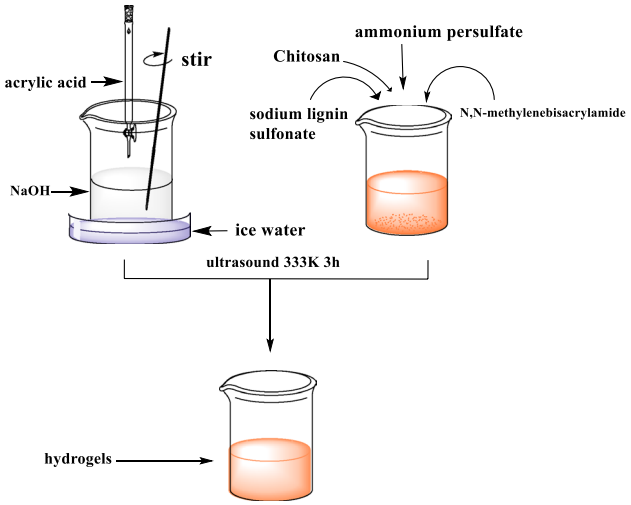

Fig. 1 Hydrogel synthesis schematic

2.3 Measurement of Swelling Properties of the Hydrogel

A certain quality of the dry sample was immersed in aqueous solution such as deionized water until the swelling behavior

was achieved a balance at room temperature. The swollen sample was then filtered through a 120-mesh nylon tea bag to take carefully out the unabsorbed water, which next was stood for 10 min to ensure that the weight of hydrogel was unconverted. The water absorbency of hydrogels were calculated by the following equation:

$$Q_e = \frac{m_2 - m_1}{m_1} \quad (1)$$

where m_1 (g) and m_2 (g) represent the weight of the dry sample and swollen sample, respectively. Q_e (g g^{-1}) was calculated as grams of water per gram of sample. Measurements were carried out three times for all samples and the average results were shown in the paper.

2.4 Measurement of Adsorption Properties of the Hydrogel

A certain amount of dry sample was added to 50 ml 250 mg/L Co^{2+} solution and 50 ml 250 mg/L Cu^{2+} solution, respectively, which had been prepared. Then placed in a thermostatic shaker until adsorption equilibrium was reached absolutely. The residual Co^{2+} concentration and Cu^{2+} concentration in the solution were measured with a TAS-986 atomic absorption spectrophotometer. The hydrogel adsorption capacity was calculated by the following equation:

$$q_e = \frac{(C_o - C_e)V}{M} \quad (2)$$

C_o (mg L^{-1}) and C_e (mg L^{-1}) represent the initial concentration and equilibrium concentration of heavy metal ions in the solution, q_e (mg g^{-1}) is the adsorption capacity of heavy metal ions on the adsorbent, the volume of solution and the weight of adsorbent were used for M (g).

2.5 Characterization of the PVA-P (AA-co-AM)

The Fourier-transform Infrared(FT-IR)spectra of samples were measured using a Nicolet Nexus 470 spectrometer (Nicolet, USA) in the wavenumber range of 400–4000 cm^{-1} by the KBr-disk method that a quality of samples were thoroughly ground with dried KBr (mass ratio ≈ 1:100) .

The micro-morphology analysis of samples were studied using a field emission Scanning Electron Microscope (SEM) JSM-7001F (Jeol Ltd, Japan). The dried samples were covered with a layer gold and imaged at an accelerating voltage of 15.0 kV.

The thermogravimetric analysis (TGA) of samples were evaluated using an STA 449C integrated thermal analyzer (Netzsch, Germany) with a heating rate of 5 °C min^{-1} from 20 °C to 800 °C in a nitrogen atmosphere.

Table 2 The results of L_9 (4^3) experiment

$L_9(4^3)$	Factors				Water absorbent rate (g g^{-1})
	A	B	C	D	Deionized water/Q_e
1	A_1	B_1	C_1	D_1	986
2	A_1	B_2	C_2	D_2	643
3	A_1	B_3	C_3	D_3	418
4	A_2	B_1	C_2	D_3	818
5	A_2	B_2	C_3	D_1	607
6	A_2	B_3	C_1	D_2	770
7	A_3	B_1	C_3	D_2	750
8	A_3	B_2	C_2	D_3	527
9	A_3	B_3	C_1	D_1	405

Table 3 The range analysis of the L_9 (4^3) experimental results

Analysis	A	B	C	D
k_1	682.33	851.33	761	666
k_2	731.67	592.33	622	721
k_3	560.67	531	591.67	587.67
R	171	320.33	169.33	133.33
Optimal level	A_2	B_1	C_1	D_2

3 Results and Discussion

3.1 Results and Range Analysis of Orthogonal Experiments

In the experiment, it is the use of ultrasound to accelerate the collision between liquid molecules and the cavitation effect of the free radical to synthesize the reaction. By orthogonal design to optimize the experimental conditions, resulting in the best performance of the hydrogels. The results of the orthogonal experiments were shown in Table 2, where each Q_e is the average of the experiments. Table 3 for the orthogonal test results of the intuitive analysis, it can be drawn from Table 3, the main impact of the size of the relationship between factors: amount of initiator > amount of linker > amount of CTS > SLS / AA mass ratio. Therefore, the optimal ratio of $A_2B_1C_1D_2$ was obtained, thus a new sample was synthesized, and its magnification of absorbing deionized water was 1120 g g^{-1}.

3.2 Characterization Analysis of the Hydrogel

3.2.1 SEM

As shown in Fig. 2, the different parts of the experimental hydrated samples were observed under different

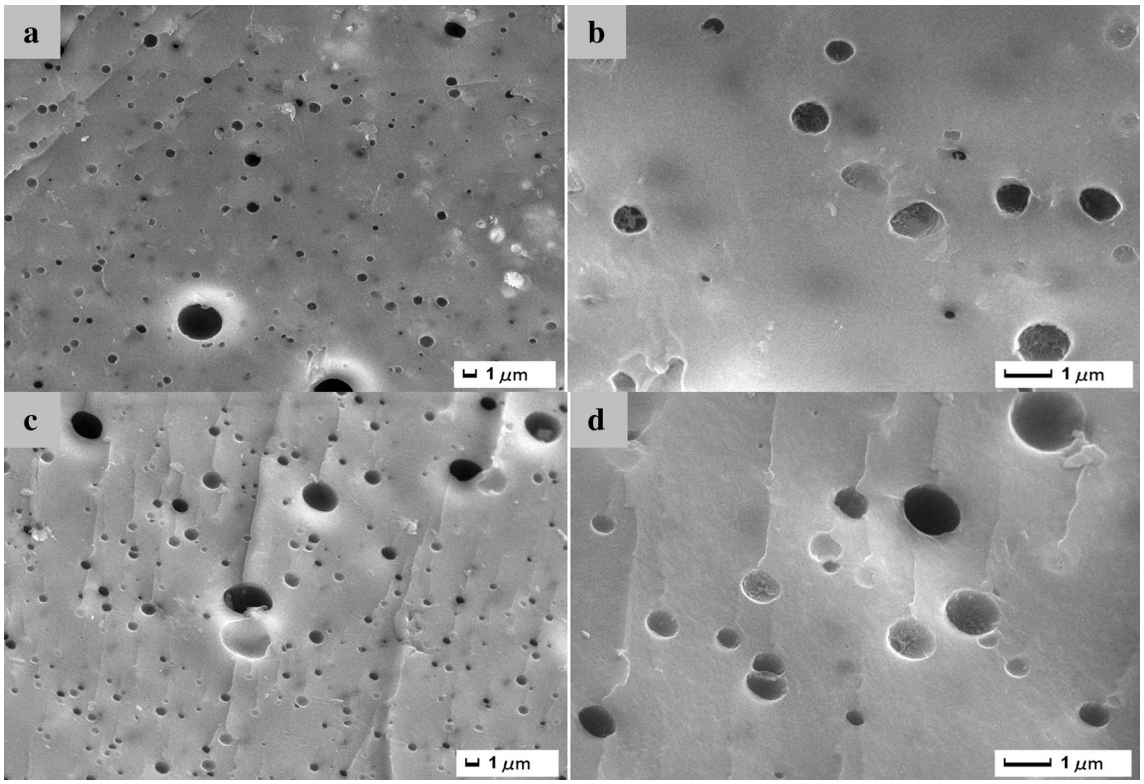

Fig. 2 Lignin-based hydrogel scanning electron micrograph

magnifications scanning electron microscope. From the figure we can clearly see that the surface of sample has holes of different sizes, uneven distribution and the depths of the hydrogels are also different. It can also be observed from Fig. 2a and c that the surface of the hydrogel has folds. The surface structure of all the folds and holes determines the large specific surface area and the effective contact area of the hydrogels so that the hydrogels adhesive greatly enhance the adsorption capacity. In summary, it shows that the experiment has successfully obtained hydrogel.

3.2.2 FT-IR

Figure 3 shows infrared spectra of lignin-based hydrogel (a), chitosan (b) and sodium lignosulfonate (c). In the infrared spectrum of chitosan (b), the peak of –OH absorption at 3580 cm^{-1}, the stretching vibration of $–NH_2$ at 2908 cm^{-1}, the bending vibration peak of $–NH_2$ at 1683 cm^{-1}, the peak at 1509 cm^{-1} And 1057 cm^{-1} ether bond absorption band, 770 cm^{-1} at a typical C-H bending vibration peak; sodium lignosulfonate (c) the main characteristic absorption peaks are: 3414 cm^{-1} at the hydroxyl O–H stretching vibration peak at 2927 cm^{-1} for the C–H stretching vibration band, the two strong absorption peaks at 1586 cm^{-1} and 1239 cm^{-1} are typical aromatic ring absorption vibration peaks at

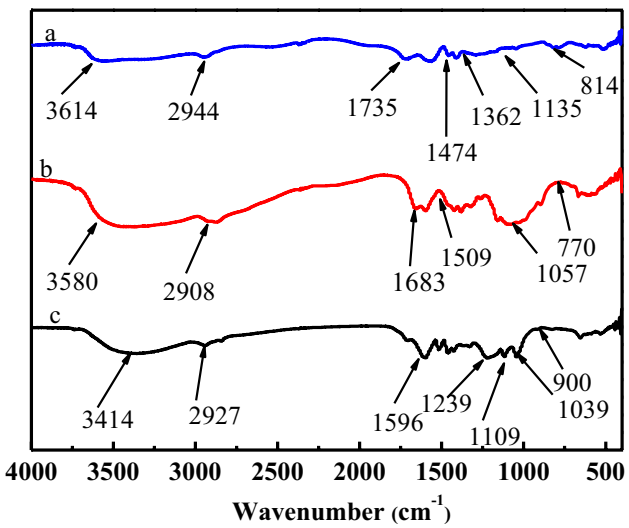

Fig. 3 FT-IR image of lignin-based hydrogel (**a**), chitosan (**b**) and sodiumlignosulfonate (**c**)

1109 cm^{-1} S=O antisymmetric Stretching vibration peak, the strong absorption peak at 1039 cm^{-1} is $–SO_3^-$ asymmetric stretching vibration peak at 900 cm^{-1} is the S-O absorption vibration peak; curve a, lignin-based hydrogel samples at 3614 cm^{-1} A strong absorption peak of –OH appeared at 2944 cm^{-1} and 1735 cm^{-1}, respectively. The aromatic ring

absorption peak at 1474 cm^{-1} show aromatic ring structure at 1374 cm^{-1}, 1135 cm^{-1} and 814 cm^{-1} at the sulfonic acid group characteristic absorption peak. In summary, experiments using chitosan and sodium lignosulfonate have been successfully prepared lignin-based hydrogel.

3.2.3 TG/DTG

Figure 4 shows the thermogravimetric plot of sodium lignosulphonate, chitosanand the hydrogels prepared experimentally, where TG is the thermogravimetric curve and DTG is the differential thermogravimetric analysis curve for the corresponding TG. The thermal decomposition of sodium lignosulfonate mainly consists of three stages, the first stage (43.3 °C–149.9 °C), from the figure we can see that this stage pyrolysis rate is slower, mainly free water and combined water evaporation; the second stage occurs between 149.9 °C and 241.1 °C. This stage is mainly the process of depolymerization of sodium lignosulfonate with weightlessness and vitrification. The third stage occurs between 241.1 °C and 442.3 °C. Within this temperature range, the lignin sulfonate heat loss is the most obvious, at 272.5 °C, the rate of weight loss reach the highest, at this time the volatiles account for about 45% of its total amount, is the most important phase of lignin sulfonate pyrolysis. The thermogravimetric analysis of chitosan showed that when the temperature reached 55.1 °C, the chitosan begin to lose weight and take the water off. Under the temperature range of 260.3 °C–343.7 °C, the weight loss of chitosan was the most obvious. At 308.3 °C, the thermal decomposition rate of chitosan reached the maximum. Thermal analysis of the hydrogel samples showed that the hydrogel begin to lose moisture at 86.7 °C, and the weight loss rate was relatively slow. When the temperature reached 454 °C, the weight loss rate reached the maximum. It can be shown that compared with sodium lignosulphonate and chitosan, lignin-based hydrogels synthesized from them have higher thermal stability.

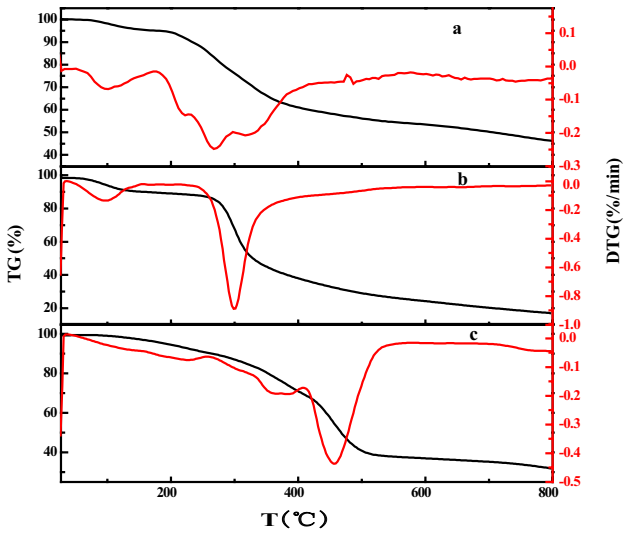

Fig. 4 Thermogravimetric analysis of sodium lignosulfonate (**a**), chitosan (**b**) and lignin based hydrogel (**c**)

3.3 Study on the Properties of Hydrogel

3.3.1 Effect of pH on the Absorption Capacity of Hydrogel

As can be seen in Fig. 5, the pH of the solution is in the range of 1–6. As the pH increasing, the amount of metal ions also increases. From this, it can be seen that under acidic conditions, supramolecular hydrogel adsorption capacity is stronger. This is due to the following balance in solution:

$$R - NH_3^+ \leftrightarrow R - NH_2 + H^+$$

$$R - NH_2 + Me^{2+} \leftrightarrow R - NH_2Me$$

Lignin-based hydrogels contain $–NH_2$, which under acidic conditions, combines with H^+ in solution to form a cationic group, $–NH_3^+$, hindering similarly charged metal ions from moving closer to the molecular chain, while H^+ also competes with heavy metal ions adsorption site, resulting in reduced hydrogel adsorption capacity.

3.3.2 Effect of Reaction Time on the Adsorption Capacity of Hydrogel

Figure 6 shows that when the reaction time is within 0–60 min, the adsorption capacity of hydrogel rapidly increases with the increase of reaction time. When the reaction time is between 60–80 min, the adsorption capacity of hydrogel to Co^{2+} gradually increased with the reaction time and tended to balance. While the adsorption amount of Cu^{2+}

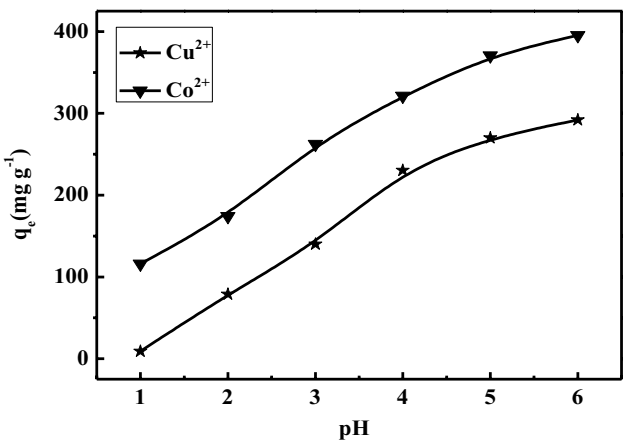

Fig. 5 Amount of metal ions adsorbed by hydrogels at different pH

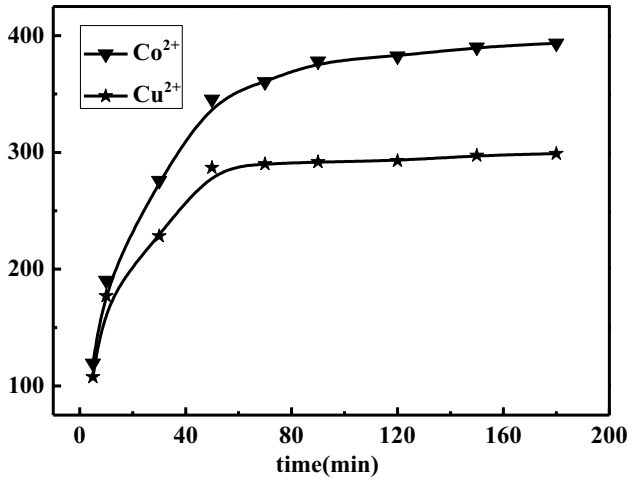

Fig. 6 Amount of metal ions adsorbed by hydrogels at different reaction times

no longer changed, it indicates that the adsorption of Cu^{2+} has reached saturation. When the reaction time reached more than 80 min, the adsorption capacity of Co^{2+} also basically no longer change, indicating that the adsorption of Co^{2+} also has reached saturation.

3.3.3 Effect of Adsorbent Dosage on the Adsorption Capacity of Hydrogel

As shown in Fig. 7 in other conditions remain unchanged, when the amount of adsorbent in the range of 0–0.015 g, the increase in the amount of adsorbent solution is conducive to the adsorption of hydrogel. Within this range, the adsorbent will provide more sites for adsorption as the amount of adsorbent increases, resulting in an increase in the amount of adsorbed hydrogel. When the amount of adsorbent exceeds 0.015 g, the amount of adsorbed hydrogel decreases with the increase of the amount of adsorbent, which is probably because the amount of adsorbent is very high, however, the concentration of metal ions is still unchanged, resulting in many of the adsorption sites in the hydrogel because there is not enough metal ions combined with them in an unsaturated state. At the same time, the solution containing high levels of adsorbent cause the role of aggregation between them, resulting in a large number of empty adsorption sites, resulting in the adsorption of hydrogel decreased. It can also be observed from the figure that the adsorption capacity of hydrogel is the best when the adsorbent dosage is up to 0.015 g, no matter Cu^{2+} or Co^{2+}. Among them, the adsorption capacity of Co^{2+} is 385 mg g^{-1} and Cu^{2+} is 290 mg g^{-1}.

3.3.4 Effect of Initial Concentration of Metal Ions on the Absorption Capacity of Hydrogel

Figure 8 shows that the adsorption of both ions by the lignin-based hydrogel increases with the initial concentration of metal ions within the experimental range when the other reaction conditions are not changed, and its adsorption capacity for Co^{2+} better than Cu^{2+}. The results show that the amount of the hydrogel adsorbed in a concentration-dependent manner. When the concentration of metal ions increases, the mass transfer power such as ion exchange and electrostatic attraction between solid and liquid phases also increases, which makes the adsorption of metal ions are more likely to overcome resistance.

3.4 Adsorption Kinetics on Co^{2+} Ions and Cu^{2+} Ions

Figures 9a and 10a show the effect of contact time on the adsorption capacity of hydrogels to Co^{2+} ions or Cu^{2+} ions.

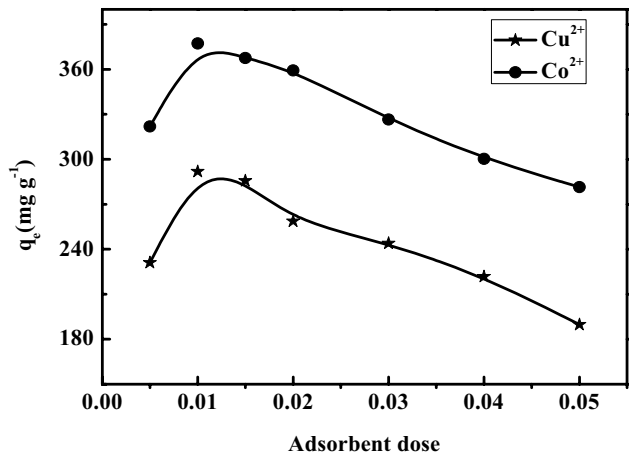

Fig. 7 Amount of metal ions adsorbed by hydrogels at different adsorbent loadings

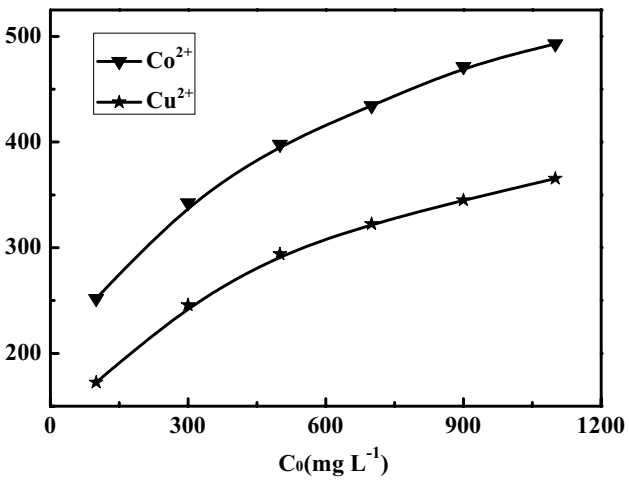

Fig. 8 Amount of adsorbed hydrogels at different initial concentrations of metal ions

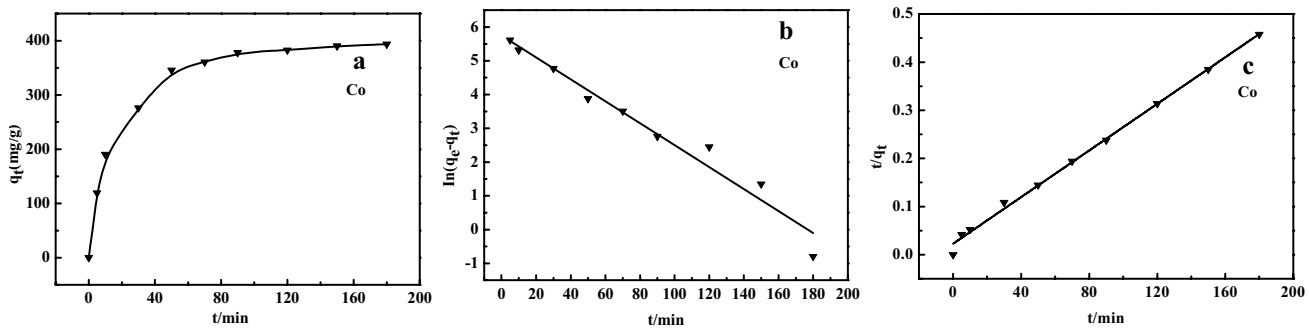

Fig. 9 **a** Effect of contact time on the Co^{2+} ions adsorption. **b** Pseudo-first-order kinetic model. **c** Pseudo-second-order kinetic model

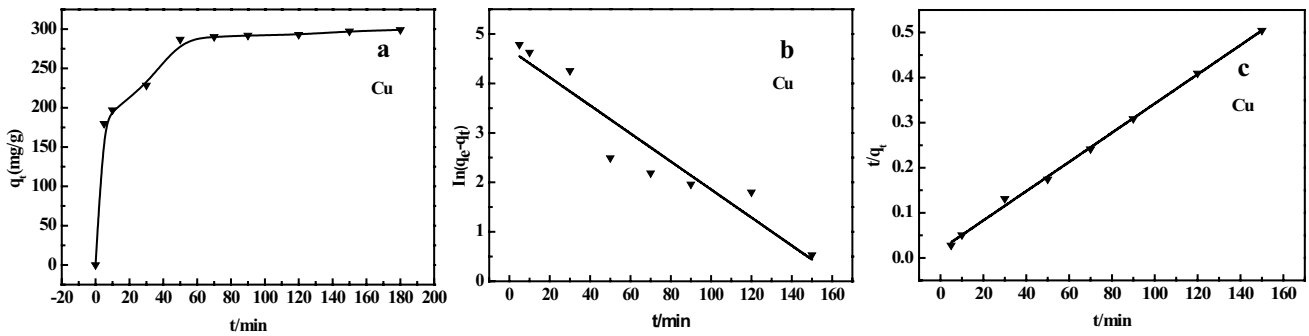

Fig. 10 **a** Effect of contact time on the Cu^{2+} ions adsorption. **b** Pseudo-first-order kinetic model. **c** Pseudo-second-order kinetic model

It can be concluded from the figure that the adsorption speed at the beginning is very high, and the adsorption rate decreases gradually with time until it reaches a steady state. The reason for this phenomenon is that as the time increases, the adsorption site gradually decreases, the resistance of heavy metal ions entering the hydrogel begins to increase, resulting in a decrease in speed. Adsorption kinetics model is usually used to describe the adsorption rate, in this experiment it was used two kinetic models: pseudo-first-order and pseudo-second-order. The adsorption mechanism of hydrogels on heavy metal ions adsorption was discussed by data processing of kinetic model. The data obtained from time were plotted in the pseudo-first-order and pseudo-second-order kinetic models b and c in Figs. 9 and 10, respectively. The equations for the two kinetic models are:

$$\ln(q_e - q_t) = \ln q_e - k_1 t \tag{3}$$

$$\frac{t}{q_t} = \frac{1}{k_2 q_e^2} + \frac{t}{q_e} \tag{4}$$

where q_e represents the adsorption capacity at equilibrium, q_t represents the amount of heavy metal ions adsorbed at time t, k_1 and k_2 are the rate constants for the pseudo-first-order and pseudo-second-order kinetic models, respectively, and two ion adsorption kinetics fitting parameters powers are listed in Tables 4 and 5. It can be concluded from the results that the correlation coefficient (R^2) of the pseudo-second-order kinetic model is higher than that of the pseudo-first-order kinetic model (R^2). In addition, the theoretical maximum adsorption (q_e) calculated by the pseudo-second-order kinetic model is closer to the experimental results than the pseudo-first-order kinetic model. Therefore, the adsorption

Table 4 Adsorption kinetic parameters-Co^{2+} ions

Pseudo-first-order kinetic model		Pseudo-second-order kinetic model	
k_1 (min^{-1})	0.03252	k_2 (g mg^{-1} min^{-1})	0.000256
q_e (mg g^{-1})	315.06	q_e (mg g^{-1})	413.22
R^2	0.9609	R^2	0.99582

Table 5 Adsorption kinetic parameters-Cu^{2+} ions

Pseudo-first-order kinetic model		Pseudo-second-order kinetic model	
k_1 (min^{-1})	0.02835	k_2 (g mg^{-1} min^{-1})	0.00324
q_e (mg g^{-1})	108.78	q_e (mg g^{-1})	308.64
R^2	0.89828	R^2	0.99793

process is more in line with the pseudo-second-order kinetic model. It shows that the adsorption of heavy metal ions on the hydrogel is chemisorption.

3.5 Adsorption Isotherm on Co^{2+} Ions and Cu^{2+} Ions

Figures 11a and 12a respectively show the influence of the initial concentration on the adsorption of hydrogel on Co^{2+} ions and Cu^{2+} ions. Both plots show that as the initial concentration increases, the amount of adsorption increases. This also explains that the concentration gradient increases with increasing initial concentration. The isotherm model was used to analyze the interaction between the molecules and the adsorbent surface. Two common adsorption isotherm models (Langmuir and Freundlich adsorption isotherm models) were used to analyze the adsorption of both ions. Use the two models to draw a curve with the initial concentration as the independent variable. Figure 11b and c are two adsorption models of Co^{2+} ions, and Fig. 12b and c are two adsorption models of Cu^{2+} ions. The equations for these two adsorption models are as follows:

$$\frac{c_e}{q_e} = \frac{1}{K_L q_m} + \frac{c_e}{q_m} \tag{5}$$

$$\ln q_e = \ln K_f + \frac{1}{n} \ln c_e \tag{6}$$

q_e (mg g^{-1}) and C_e (mg L^{-1}) are the adsorption amount and concentration of metal ions in solution at equilibrium, respectively. q_m (mg g^{-1}) is the theoretical maximum adsorption capacity. K_L and K_f are the constants of the Langmuir and Freundlich isotherm models, respectively, and n is the heterogeneity factor. The parameters for the Langmuir and Freundlich isotherms were listed in Table 6. It can be concluded from the data in Table 6 that the Freundlich isotherm

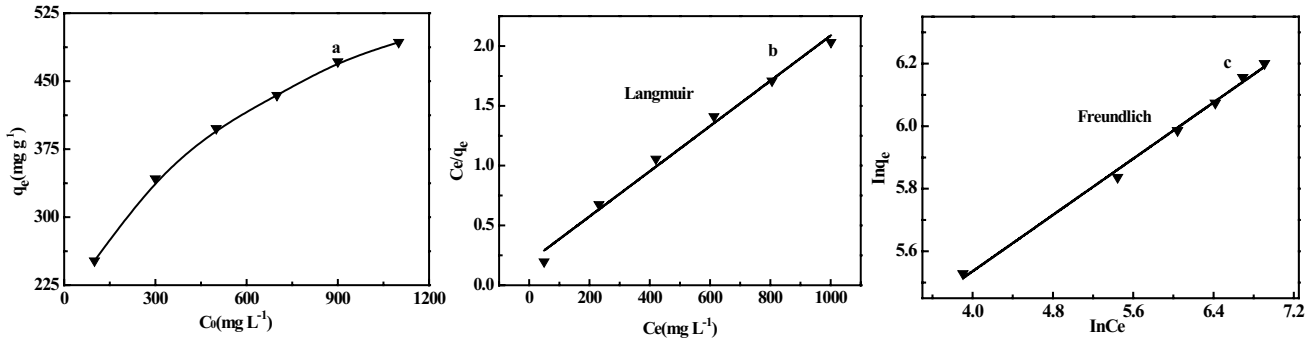

Fig. 11 **a** Effect of initial concentration on the Co^{2+} ions adsorption; **b** Langmuir isotherm model. **c** Freundlich isotherm model

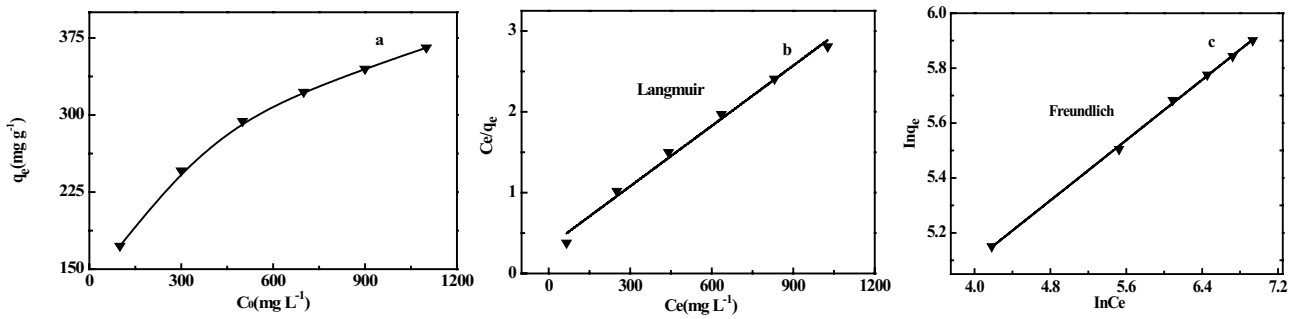

Fig. 12 **a** Effect of initial concentration on the Cu^{2+} ions adsorption; **b** Langmuir isotherm model. **c** Freundlich isotherm model

Table 6 Adsorption isotherms parameters

Isotherm models	Langmuir model			Freundlich model		
Parameters	q_m (mg g^{-1})	K_L (L mg^{-1})	R^2	K_F (L g^{-1})	1/n	R^2
Cu^{2+}	401.6	0.00750	0.99016	54.59	0.2746	0.99899
Co^{2+}	529.1	0.00959	0.98838	103.2	0.2248	0.99502

model is closer to the ion adsorption process, whereas the Langmuir isotherm model is difficult to describe the ion adsorption process. This shows that the process of hydrogel adsorption of two heavy metal ions is multi-layer adsorption.

4 Conclusion

In this paper, we successfully prepared high-performance hydrogel by ultrasonic assisted method and optimized the optimal hydrogel by orthogonal design. Hydrogel has excellent swelling properties, reaching 1120 g g^{-1} in deionized water. The results show that the hydrogel has good adsorption properties for cobalt ions and copper ions. At pH 6, the amount of adsorbent was 0.015 g, the adsorption was about 80 min, and the higher the initial concentration of heavy metal ions, the stronger the adsorption ability of hydrogel. Adsorption process is used for chemical adsorption, to meet the multi-layer adsorption. In conclusion, hydrogels with many excellent properties will have great application prospects in wastewaters and heavy metal pollution treatment.

References

1. F. Wang, Y. Pan, P. Cai, T. Guo, H. Xiao, Bioresour. Technolo. **241**, 482–490 (2017)
2. B. Xiang, W. Fan, X. Yi, Z. Wang, F. Gao, Y. Li, H. Gu, Carbohydr. Polym. **136**, 30–37 (2016)
3. R. Slimani, I.E. Ouahabi, A. Elmchaouri, B. Cagnonc, S.E. Antri, S. Lazar, Chem. Data Collections **9–10**, 184–196 (2017)
4. Z. Dong, F. Zhang, D. Wang, X. Liu, J. Jin, J. Solid State Chem. **224**, 88–93 (2015)
5. X. Liu, D.J. Lee, Bioresour. Technol. **160**, 24–31 (2014)
6. N. Maaloula, P. Oulegob, M. Rendueles, A. Ghorbal, M. Díaz, J. Environ. Chem. Eng. **5**, 2944–2954 (2017)
7. T. Liu, X. Han, Y. Wang, L. Yan, B. Du, Q. Wei, D. Wei, J. Colloid. Interf. Sci. **508**, 405–414 (2017)
8. R. Wang, W. Wang, H. Ren, J. Chae, Biosens. Bioelectron. **57**, 179–185 (2014)
9. N.P. Raval, P.U. Shah, N.K. Shah, J. Environ. Manage. **179**, 1–20 (2016)
10. A.S. Singha, A. Guleria, Int. J. Biol. Macromol. **67**, 409–417 (2014)
11. Y. Cui, Q. Ge, X.Y. Liu, T.S. Chung, J. Membrane Sci. **467**, 188–194 (2014)
12. M. Šæiban, M. Klašnja, B. Škrbiæ, Desalination **229**, 170–180 (2008)
13. G. Zeng, J. Wan, D. Huang, L. Hua, C. Huang, M. Cheng, W. Xue, X. Gong, R. Wang, D. Jiang, J. Hazard. Mater. **339**, 354–367 (2017)
14. A.A. El-Bayaa, N.A. Badawy, E.A. AlKhalik, J. Hazard. Mater. **170**, 1204–1209 (2009)
15. Y.L. Han, Y.C. Lo, C.L. Cheng, W.J. Yu, D. Nagarajan, C.H. Liu, Y.H. Li, J.S. Chang, Biochem. Eng. J. **117**, 48–56 (2017)
16. A.R. Keshtkar, A. Tabatabaeefar, A.S. Vaneghi, M.A. Moosavian, J. Environ. Chem. Eng. **4**, 1248–1258 (2016)
17. K. Mizoguchi, J. Ida, T. Matsuyama, H. Yamamoto, Sep. Purif. Technol. **75**, 69–75 (2010)
18. Q. Zhu, Z. Li, Chem. Eng. J. **281**, 69–80 (2015)
19. H. Liu, C. Wang, J. Liu, B. Wang, H. Sun, J. Environ. Manage. **128**, 727–734 (2013)
20. M.A. Abdel-Khalek, M.K. Abdel Rahman, A.A. Francis, J. Environ. Chem. Eng. **5**, 319–327 (2017)
21. L. Zheng, C. Zhu, Z. Dang, H. Zhange, X. Yi, C. Liu, Carbohydr. Polym. **90**, 1008–1015 (2012)
22. W. Zhang, Y. Zhang, Y. Gutha, X. Jiao, Int. J. Biol. Macromol. **105**, 422–430 (2017)
23. A. Witek-Krowiak, D.H.K. Reddy, Bioresour. Technol. **127**, 350–357 (2013)
24. S. Yuan, P. Zhang, Z. Yang, L. Lv, S. Tang, B. Liang, Int. J. Biol. Macromol. **109**, 287–302 (2018)
25. T. Song, C. Yu, X. He, J. Lin, Z. Liu, X. Yang, Y. Zhang, Y. Huang, C. Tang, Colloids Surf. A **537**, 508–515 (2018)
26. M.A. Barakat, J. Colloid Interface Sci. **291**, 345–352 (2005)
27. H.M. Albishri, H.M. Marwani, J. Chem. **9**, S252–S258 (2016)
28. P.D. Chethan, B. Vishalakshi, Int. J. Biol. Macromol. **75**, 179–185 (2015)
29. T.A.H. Nguyen, H.H. Ngo, W.S. Guo, J. Zhang, S. Liang, Q.Y. Yue, Q. Li, T.V. Nguyen, Bioresour. Technol. **148**, 574–585 (2013)
30. A.O. Dada, F.A. Adekola, E.O. Odebunmi, Environ. Nanotechnol. Monitor. Manage. **8**, 63–72 (2017)
31. G. Vázquez, M.S. Freire, J. González-Alvarez, G. Antorrena, Desalination **249**, 855–860 (2009)
32. P.G. González, Y.B. Pliego-Cuervo, Chem. Eng. Res. Des. **92**, 2715–2724 (2014)
33. A. Abdolali, H.H. Ngo, W. Guo, S. Lu, S.S. Chen, N.C. Nguyen, X. Zhang, J. Wang, Y. Wu, Sci. Total Environ. **542**, 603–611 (2016)
34. R.K. Gautam, A. Mudhoo, G. Lofrano, M.C. Chattopadhyaya, J. Environ. Chem. Eng. **2**, 239–259 (2014)
35. S. Kheirandish, M. Ghaedi, K. Dashtian, R. Jannesar, M. Montazerozohori, F. Pourebrahim, M.A. Zare, J. Colloid Interface Sci. **500**, 241–252 (2017)
36. K. Kesenci, R. Say, A. Denizli, Eur. Polym. J. **38**, 1443–1448 (2002)
37. E. Fosso-Kankeu, H. Mittal, F. Waanders, S.S. Ray, J. Ind. Eng. Chem. **48**, 151–161 (2017)
38. J.T. Tsiepe, B.B. Mamba, A.S. Abd-El-Aziz, A.K. Mishra, J. Inorg. Organomet. Polym. Mater. **28**, 467–480 (2018)
39. J. Yang, Z. Li, H. Zhu, Appl. Catal. B **217**, 603–614 (2017)
40. H. Xie, Z. Zhao, S. An, Y. Jiang, Colloid Surf. B **136**, 1113–1119 (2015)